Deuterium NMR Relaxation Studies of Peptide–Lipid Interactions†

R. Scott Prosser and James H. Davis*

Department of Physics, University of Guelph, Guelph, Ontario, Canada N1G2W1

Christian Mayer, Klaus Weisz, and Gerd Kothe

Institut für Physikalische Chemie, Universität Stuttgart, Pfaffenwaldring 55, D-7000 Stuttgart 80, Germany

Received April 9, 1992; Revised Manuscript Received July 9, 1992

ABSTRACT: A unique model membrane system composed of a synthetic amphiphilic peptide (Lys_2-Gly-Leu_{16}-Lys_2-Ala-amide) and a specifically labeled phospholipid (1,2-[7,7-$^2H_2$]dipalmitoyl-*sn*-glycero-3-phosphocholine) has been studied by ^2H NMR, using inversion recovery, quadrupolar echo, and modified Jeener-Broekaert sequences, from 213 to 333 K, at molar peptide concentrations of 0, 2, 4, and 6%. Analysis of the experiments, employing a density matrix treatment based on the stochastic Liouville equation, revealed information about the dynamic organization of the lipid in the model membrane system, whose phase behavior has been determined previously [Huschilt et al. (1985) *Biochemistry 24*, 1377–1386]. The dynamic organization is described in terms of segmental and molecular order parameters and in terms of correlation times corresponding to both internal and overall lipid motions. In the liquid crystalline phase, the molecular order parameter, S_{ZZ}, was observed to decrease slightly upon addition of peptide while the conformational order parameter corresponding to the seventh segment, $S_{Z'Z'}$, did not change for any concentration of peptide. In general, the gauche–trans isomerization rate in the middle of the chain was not observed to change upon peptide addition, whereas the whole body reorientational correlation times ($\tau_{R_\parallel}$ and $\tau_{R_\perp}$) increased by nearly an order of magnitude. The anisotropy ratio ($\tau_{R_\perp}/\tau_{R_\parallel}$) decreased with peptide added. An additional motion which involves a jump about the axis of the *sn*-2 chain is also observed to be slowed down significantly in the presence of peptide. Assuming T_2 is dominated by order director fluctuations in the liquid crystalline phase, we conclude that peptide decreases the effective membrane elastic constant. In the gel state, the jumping process of the *sn*-2 chain is observed to slow down slightly while the whole body correlation times ($\tau_{R_\parallel}$ and $\tau_{R_\perp}$) decrease with peptide added. In one sense, the peptide serves to decrease the differences between the fluid and gel states.

The biological plasma membrane is a complex molecular assembly whose many components influence the structural and dynamic properties of each other and of the system as a whole. A comprehensive study of such a system must therefore reflect the microscopic properties of the individual components (conformation, local and molecular order, and internal and whole body dynamics), the mesoscopic properties of membrane domains (features of surface undulations or defects associated with a lipid annulus about a protein), and properties of the assembly (overall physical properties like bilayer separation, elastic constants, viscosity, and phase equilibria).

We have chosen to employ a model membrane consisting of 1,2-dipalmitoyl-*sn*-glycero-3-phosphocholine (DPPC) and a synthetic amphiphilic polypeptide, with the sequence Lys_2-Gly-Leu_{16}-Lys_2-Ala-amide (peptide-16), in order to study the above features. By employing circular dichroism, differential scanning calorimetry (DSC), low-angle X-ray diffraction, and ^1H and ^2H nuclear magnetic resonance (NMR), the secondary structure of the peptide, bilayer dimensions, and phase equilibria of the model membrane were determined (Davis et al., 1983; Huschilt et al., 1985). The order and dynamics of peptide-16 in a phospholipid bilayer have also been studied by both ^2H (Pauls et al., 1985; (J. H. Davis, X. Shan, D. B. Langlais, M. Auger, and B. Griffin, unpublished results, 1991) and ^{13}C NMR (J. H. Davis, X. Shan, M. Auger, and B. Griffin, private communication). Morrow and Whitehead (1988) have carried out a Landau expansion of the free energy in terms of area per lipid in order to obtain protein–lipid phase diagrams with critical mixing and a maximum peptide concentration for phase separation. Their simulations reproduce experimentally obtained partial phase diagrams and certain features of the DSC profiles as a function of peptide concentration. In this paper, we will focus on a more microscopic level in order to consider the effect of peptide concentration on phospholipid segmental and molecular order parameters and on internal and whole body membrane phospholipid dynamics. We will present results from ^2H NMR relaxation experiments of macroscopically unoriented bilayers at four concentrations of peptide, in DPPC, specifically deuteriated at the 7-position, on both the *sn*-1 and *sn*-2 chains. The results, referring to three lipid phases and a peptide–lipid two-phase region, will be discussed in terms of other studies of membrane systems and protein–lipid interactions.

EXPERIMENTS AND METHODS

Syntheses and *Sample Preparation.* DPPC, specifically deuteriated at the 7-position of the *sn*-1 and *sn*-2 chains, was synthesized using a procedure similar to that of Gupta et al. (1977). Peptide-16 was synthesized by R. S. Hodges at the University of Alberta (Edmonton, Alberta, Canada). Samples were prepared by first codissolving peptide-16 with DPPC in methanol. After removal of the solvent by rotary evaporation, 50 mM phosphate buffer (pH 7.0) was gently stirred into the dry mixture at a weight ratio of strictly 4/3 (buffer/lipid). DSC and thin-layer chromatography (TLC) were routinely performed on each sample to characterize sample integrity. A typical NMR sample contained roughly 100 mg of lipid.

† This work has been supported by grants from the Natural Sciences and Engineering Research Council of Canada.

0006-2960/92/0431-9355$03.00/0

^2H NMR Experiments. ^2H NMR experiments were performed on a homemade spectrometer operating at 55 MHz (8.5 T), using quadrature detection. Great care was also taken to ensure that all of the signal appeared in one detecting channel; this channel was then zeroed to improve the S/N ratio (Davis, 1983). Relaxation measurements included quadrupole echo ($(\pi/2)_x$–τ_1–$(\pi/2)_y$), inversion recovery ($(\pi)_x$–τ_2–$(\pi/2)_x$–τ_1–$(\pi/2)_y$), and modified Jeener-Broekaert ($(\pi/2)_x$–τ_3–$(\pi/4)_y$–τ_4–$(\pi/4)_y$–τ_1–$(\pi/2)_y$) sequences, using appropriate phase cycling schemes. Typically between 4000 and 8000 scans were accumulated with a refocusing time, τ_1, equal to 35 μs and a repetition time of 250 ms (except below 250 K where the inversion recovery time becomes long). The parameter, τ_3, used to create quadrupolar order was set such that $\omega_Q\tau_3 = \pi/2$, thus exciting quadrupolar order for those components of the powder in which the axis of motional averaging was perpendicular to the principal magnetic field (this excitation was made more selective by the use of phase cycling strategies). The duration of a π pulse was typically 5.5 μs using a 10-mm diameter solenoid coil with 10 turns.

NMR Relaxation Model. Analysis of the dynamic ^2H NMR experiments is achieved in terms of the density operator formalism (Müller et al., 1985; Meier et al., 1986). In order to describe the time evolution of the density matrix $\rho(t)$ during some arbitrary pulse sequence, the time period is divided into regions where a pulse is present and regions where there is no pulse. The action of the different nonselective pulses is considered by unitary transformations employing Wigner rotation matrices (Schwartz et al., 1982). Between the pulses, the density matrix is assumed to obey the stochastic Liouville equation (Kubo, 1969; Freed et al., 1971)

$$\frac{\partial}{\partial t}\rho(\Omega,t) = -(i/\hbar)\,\mathcal{H}^s(\Omega)\,\rho(\Omega,t) - \Gamma_\Omega[\rho(\Omega,t) - \rho_{eq}(\Omega)] \quad (1)$$

where $\mathcal{H}^s$ denotes the Hamiltonian superoperator of the spin system, which dictates the spin dynamics, Γ_Ω is the stationary Markov operator for the various random motional processes, which dictates the relaxation, and $\rho_{eq}(\Omega)$ is the equilibrium density matrix; these operators are all a function of the orientation and conformation of the molecule, specified by the Euler angles, Ω. The above equation is solved using the finite grid point method (Norris & Weissman, 1969; Kothe, 1977) in which the Markov operator is represented by a matrix, $W(\Omega_m,\Omega_n)$, whose elements give the transition rates between discrete sites of Ω.

The Markov operator includes terms for internal, overall, and collective lipid motions. The internal chain dynamics consist of gauche–trans isomerizations, which are represented by a jump process. We distinguish between the gauche–trans isomerizations and the unique gauche–gauche isomerizations of the 2-segment leading to a two-site jump of the *sn*-2 chain (Mayer et al., 1988). The time scales of these two internal motions are very different. The latter mechanism has a profound influence on the relaxation behavior of all of the labeled sites in the *sn*-2 chain, which exhibit a common T_{1Z} minimum in the gel phase (Mayer et al., 1988). The overall lipid motion is represented by anisotropic rotational diffusion of the molecule as a whole. The dynamics of the individual molecules are thus described in terms of four correlation times: $\tau_{R\parallel}$, $\tau_{R\perp}$, τ_j, and τ_{2j} which refer respectively to rotational diffusion about the long and short axes of the molecule, gauche–trans isomerizations, and an internal two-site jump of the *sn*-2 chain. Assuming a random jump process, internal motions (gauche–trans isomerizations) may be represented by (Sillescu, 1971; Mayer et al., 1990)

$$W(\Omega_m,\Omega_n) = \tau_j^{-1}[P'_{eq}(\Omega_n) - \delta_{mn}], \quad (2)$$

where $P'_{eq}(\Omega_n)$ represents the occupation probability of a particular conformation. The transition rates for the overall lipid motions are given by (Meier et al., 1986)

$$W(\Omega_m,\Omega_{m+1}) + W(\Omega_m,\Omega_{m-1}) = (3\Delta^2\tau_R)^{-1} \quad (3a)$$

$$W(\Omega_m,\Omega_n)P''_{eq}(\Omega_m) = W(\Omega_n,\Omega_m)P''_{eq}(\Omega_n) \quad (3b)$$

$$W(\Omega_m,\Omega_m) = -(3\Delta^2\tau_R)^{-1} \quad (3c)$$

where Δ denotes the angular separation between the adjacent sites, τ_R is the correlation time ($\tau_{R\parallel}$ or $\tau_{R\perp}$, and $P''_{eq}(\Omega)$ is the occupation probability of a particular orientation.

In addition to isolated motions of single molecules, collective motions of a large number of lipids may occur in the liquid crystalline phase of membranes (Rommel et al., 1988; Stohrer et al., 1991). They can be modeled as fluctuations of the instantaneous director with respect to its time-averaged orientation (Pincus, 1969, Freed, 1977). Within the hydrodynamic theory, these time-dependent deformations of the ordered structure are analyzed in terms of a broad distribution of thermally activated normal modes (de Gennes, 1974). Using a small-angle approximation, the mean square fluctuations $\langle\theta^2(q)\rangle$ and relaxation times $\tau(q)$ of the elastic modes can be written as (Marqusee et al., 1984)

$$\langle\theta^2(q)\rangle = k_BT/(d\lambda_l^2Kq^2) \quad (4a)$$

$$\tau(q) = \eta/(Kq^2) \quad (4b)$$

Here k_B, d, λ_l, K, q, and η denote the Boltzmann constant, a coherence length associated with the bilayer thickness, the long wavelength cutoff of the elastic modes, the average elastic constant of the membrane, the wave vector of mode q, and the effective viscosity, respectively. Analysis of the collective lipid motions may provide information on the viscoelastic properties of the bilayer membranes (Stohrer et al., 1991).

The equilibrium distribution P_{eq}, is described in terms of internal and external coordinates. The internal part, P'_{eq}, accounts for different conformations and the external part, P''_{eq}, for different orientations. Generally, there are only four conformational states for a particular aliphatic chain segment. The corresponding populations n_1, n_2, n_3, and n_4 may be used to set up a segmental order matrix, which on diagonalization yields the segmental order parameters $S_{Z'Z'}$ and $S_{X'X'} - S_{Y'Y'}$ (Meier et al., 1986). They express the ordering of the most ordered segmental axis and the anisotropy of that order, respectively.

The external part of the equilibrium distribution, P''_{eq}, is described in the mean field approximation, using an orienting potential such as is common in molecular theories of liquid crystals (Cotter, 1977). In the case of an axially symmetric order tensor, which is a good approximation for lipid molecules, only one adjustable parameter, A_{00}, enters the orientational distribution function

$$f(\beta) = N\exp[A_{00}D_{00}^2(0,\beta,0)] \quad (5)$$

where $D_{00}^2(0,\beta,0)$ is an element of the second rank Wigner rotation matrix. A_{00} characterizes the orientation of the lipid molecules with respect to a local director. The orientational

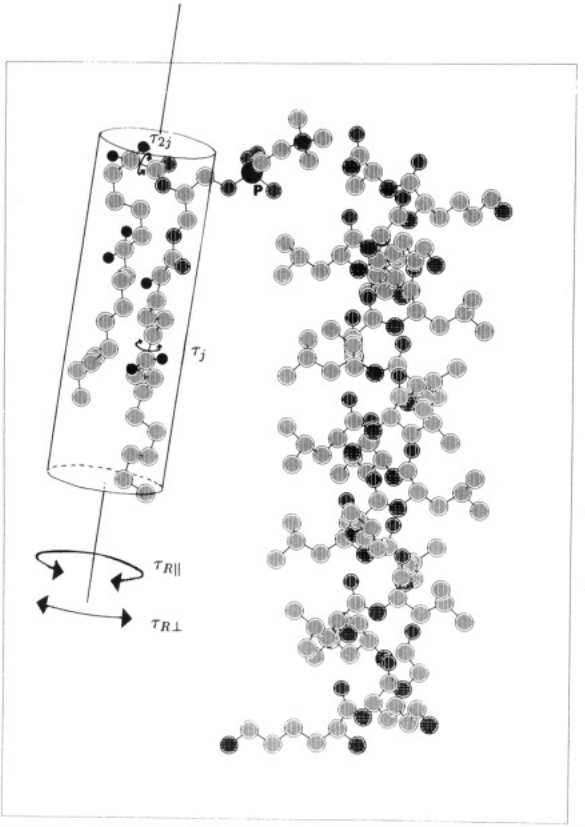

FIGURE 1: Peptide-16 alongside a fluid phase DPPC molecule. Hydrogen atoms have been omitted for clarity. Filled in balls represent deuterons; P = phosphorus; dark vertical lines represent oxygen; hatched lines represent nitrogen. $\tau_{R\perp}$, $\tau_{R\|}$, and τ_j are correlation times corresponding to overall fluctuation, overall rotation, and gauche–trans isomerization, respectively.

order parameter, S_{ZZ}, is related to the coefficient A_{00} by a mean value integral (Saupe, 1964):

$$S_{ZZ} = N\int_0^{\pi} D_{00}{}^2(0,\beta,0)\exp[A_{00}D_{00}{}^2(0,\beta,0)](\sin\beta)\,d\beta \quad (6)$$

The molecular order of the lipid molecules is thus specified by the orientational order parameter S_{ZZ} and the segmental order parameter $S_{Z'Z'}$.

Figure 1 depicts a fluid phase lipid alongside peptide-16. The phospholipid may be visualized as a spherocylinder which undergoes continuous anisotropic diffusion, characterized by $\tau_{R\|}$ and $\tau_{R\perp}$, within the above-mentioned orienting potential (eq 5). As is suggested in Figure 1, the estimated length of the peptide is such that the lipid would be expected to possess a large number of gauche conformers in order that the hydrophobic mismatch between the peptide and bilayer be minimized.

Data Analysis. The numerical integrations of the stochastic Liouville equation were achieved using the Lanczos algorithm (Moro & Freed, 1981). Within the Redfield limit, analytical solutions, based on a time-dependent perturbation treatment, were employed (Redfield, 1965). The constant parameters used in the calculations were obtained from fast rotational and rigid limit quadrupole echo spectra of the pure phospholipids. As found previously, the quadrupole coupling constant of the aliphatic deuterons is $e^2qQ/h = 169$ kHz (Meier et al., 1986).

Analysis of the ^{2}H NMR experiments requires knowledge of the various molecular tensors in the lipid systems studied. The orientation of the molecular order tensor is suggested by the geometry of the phospholipid molecule. We assume that the order tensor is axially symmetric along the phospholipid chain axis. This assumption, checked by spectral simulations of slow-motion line shapes, reflects the overall shape of the molecule, which is also expected to exhibit axially symmetric rotational diffusion along the long axis. The principal axis system of the quadrupole tensor, axially symmetric along the C–D bond, may assume four different orientations relative to the diffusion tensor. The Euler angles, characterizing these orientations, are listed elsewhere (Meier et al., 1986).

The variable parameters A_{00}, n_1, n_2, n_3, n_4, $\tau_{R\|}$, $\tau_{R\perp}$, τ_{2j}, and τ_j were determined by computer analysis of the various ^{2}H NMR experiments at any given temperature. However, they need not all be evaluated independently. In general, the gauche conformations of a particular aliphatic chain segment are assumed to be equally populated, corresponding to $n_2 = n_3$. Since $n_1 + n_2 + n_3 + n_4 = 1$, we obtain $n_2 = (1 - n_1 - n_4)/2$. Consequently, there are only two unknown populations, namely n_1 and n_4.

In the fast motional regime ($T >$ main transition temperature, T_M) the population difference $n_1 - n_4$ and $A_{00}(S_{ZZ})$ are unambiguously related to the magnitude of the quadrupole splitting $|\Delta\nu_Q|$ in the NMR spectrum by (Mayer et al., 1990)

$$|\Delta\nu_Q| = (3/4)(e^2qQ/h)|S_{CD}| \quad (7a)$$

$$S_{CD} = (1/2)S_{ZZ}(n_4 - n_1) \quad (7b)$$

thus eliminating $n_1 - n_4$ as a free parameter if S_{ZZ} is known (we are assuming that gauche–trans isomerizations are independent of whole body reorientations). As shown recently, S_{ZZ} can independently be obtained from the anisotropy of the spin lattice relaxation time (Mayer et al., 1990). Thus, the reduced line separation $|\Delta\nu_Q|/S_{ZZ}$ provides information on the conformational order at the particular labeled segment. Note that this reduced splitting only yields $n_1 - n_4$, which is insufficient for the evaluation of the complete order matrix. However, independent NMR experiments verified that $n_4 \approx 0$ for chain segments in the central part of the aliphatic chain (Meier et al., 1986).

Evaluation of the dynamic parameters $\tau_{R\|}$, $\tau_{R\perp}$, τ_{2j}, and τ_j is achieved by employing various relaxation experiments. Since the anisotropy ratio of the intermolecular motion is practically independent of temperature, $\tau_{R\perp}/\tau_{R\|}$ has to be determined only once for a particular phase. Generally, each experiment defines a specific dynamic window in which molecular motions can be studied. For instance, the spin lattice relaxation times T_{1Z} and T_{1Q} (from inversion recovery and Jeener-Broekaert sequences) are particularly sensitive to motions with correlation times $\tau \sim \omega_0^{-1}$. Thus, by employing a high magnetic field ($B = 8.5$ T), fast molecular dynamics in the range $10^{-12} - 10^{-7}$ s can be studied. In contrast, measurement of the transverse spin relaxation time T_{2E} (from quadrupole echo sequences) permits the study of much slower motions. Since T_{2E} is most sensitive to motions with correlation times $\tau_R \sim (e^2qQ/\hbar)^{-1}$, quadrupole echo sequences offer a means to study molecular dynamics in the range 10^{-7}–10^{-4} s. Generally, fast internal and overall motions of individual molecules mainly affect T_{1Z} and T_{1Q}, while T_{2E} may be dominated by slow collective order fluctuations (fluid phase) (Stohrer et al., 1991).

A useful method for characterization of motions is based on the anisotropy of the relaxation times. For macroscopically aligned bilayers, T_{1Z}, T_{1Q}, and T_{2E} vary as a function of the sample orientation. Likewise, partially relaxed NMR spectra of unoriented membranes indicate variations of the corresponding relaxation time across the powder line shape. It turns out that this variation is dependent upon the character of the motion responsible for spin relaxation (Siminovitch et al., 1988; Mayer et al., 1990; Bloom et al., 1991; Stohrer et al., 1991).

For thermally activated processes, the variation of the sample temperature can be used to separate the various types of motions. The position and absolute value of a minimum in the relaxation temperature dependence is highly indicative of the type of motion (Mayer et al., 1988). Having assigned the dominant motion in a region with such a relaxation minimum, its temperature dependence is extrapolated into other regions where the situation may be more complex. The analysis is completed if all relaxation experiments can be simulated using the same set of parameters. Thus, for example, the fit parameters for the transverse relaxation times, T_{2E}, also account for the distinctive T_{2E} anisotropy evident in the partially relaxed spectra of Figure 2. Furthermore, the fit parameters for the longitudinal relaxation times, T_{1Z} and T_{1Q}, of pure DPPC have been previously used to describe the angular dependence of these relaxation times, as described elsewhere (Mayer et al., 1990; G. Gröbner and G. Kothe, private communication).

RESULTS AND DISCUSSION

Line Shapes. Characteristic quadrupolar echo spectra are shown for the pure lipid system, in Figure 2, as a function of temperature and pulse spacing. The five selected temperatures characterize the fluid (L_α) (Figure 2A), ripple ($P_{\beta'}$) (Figure 2B), and gel ($L_{\beta'}$) (Figure 2C–E) phases of pure DPPC bilayers. The spectra of the L_α phase exhibit a narrow axially symmetric powder pattern. Cooling below T_M at 314.5 K causes drastic changes in the DPPC spectra. They now disclose broad featureless line shapes indicative of slow molecular dynamics, which gradually change to a rigid limit powder spectrum (not shown). Note the distinct T_{2E} anisotropy evident in the partially relaxed spectra at any given temperature.

Closer inspection of Figure 2B suggests that there may be two spectral components in this temperature realm. Two-component spectra of this kind have been observed before in the $P_{\beta'}$ phase (Wittebort et al., 1981; Schneider et al., 1983; Meier et al., 1983). Meier et al. observed two spectral components in DMPC, deuteriated in the methyl position of the *sn*-2 chain, and concluded that simulation of these components was only possible with two distinct molecular order parameters corresponding to the L_α and $L_{\beta'}$ phases extrapolated to the temperature of interest.

Below the main phase transition, the hydrocarbon chains are known to become generally ordered, creating a mismatch of areas in the bilayer plane between chains and headgroups (Stamatoff et al., 1982). The packing problem in these anisotropic molecules is solved by the creation of the ripple ($P_{\beta'}$) phase. Statistical mechanical treatments on the formation of this phases have been given recently (Carlson & Sethna, 1987; McCullough et al., 1990). The rippled profile suggests the possibility of defects or vacancies wherein lipids possess degrees of freedom similar to those in the liquid crystalline phase (Kapitza et al., 1984). We envision such a system comprised of both motionally restricted and unrestricted lipids, where the fraction of restricted molecules increases with decreasing temperature until only the high order component is left (at $T \approx 288$ K).

Figure 3 displays the first spectral moment, M_1, as a function of inverse temperature and peptide concentration. Here we define M_1 according to

$$M_1 = \frac{\int_0^\infty f(\nu)\nu \, d\nu}{\int_0^\infty f(\nu) \, d\nu} \qquad (8)$$

where $f(\nu)$ represents the spectrum as a function of frequency, ν, measured from the center of the spectrum. M_1, which is proportional to S_{CD} (eq 7) in the fast motional regime, is clearly not strongly dependent on peptide concentration in the L_α phase; however, significant deviations in M_1 are observed as a function of peptide concentration from T_M to 288 K. At still lower temperatures in the $L_{\beta'}$ phase, M_1, for the sample containing 2% peptide, deviates slightly from the pure lipid M_1 profile. Figure 3 also shows the two-phase regions for the systems containing 2% and 4% peptide-16 (Huschilt et al.,

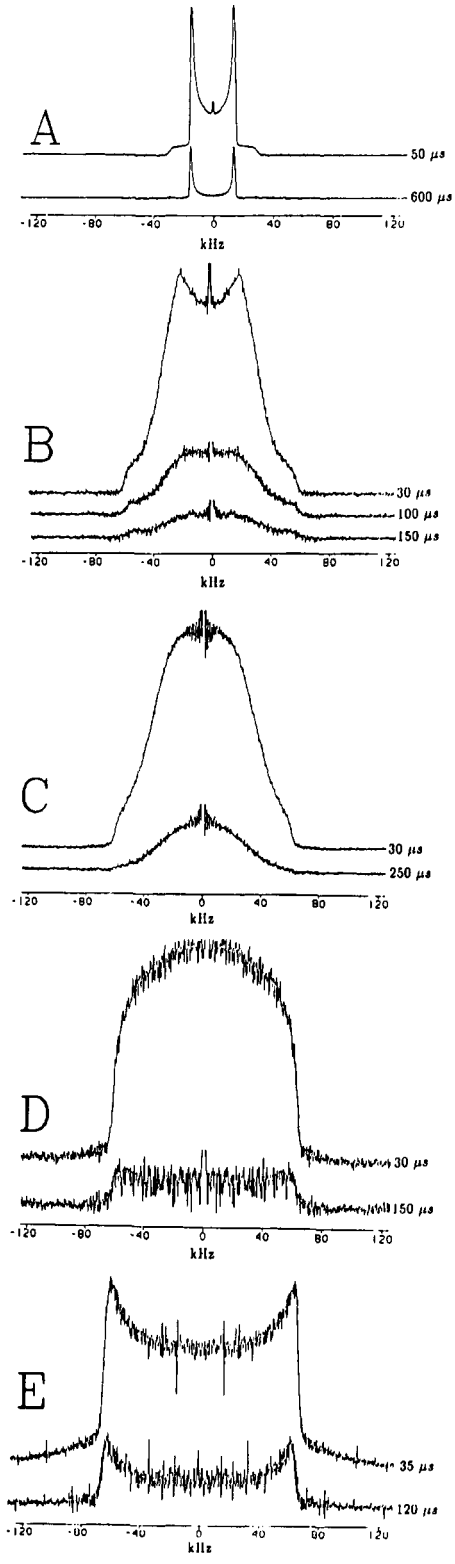

FIGURE 2: Quadrupole echo spectra of multilamellar dispersions of [7,7,-$^2H_2$]DPPC acquired at 317 K (A), 305 K (B), 288 K (C), 254 K (D), and 216 K (E). Corresponding pulse separation times (in microseconds) are shown alongside each of the spectra.

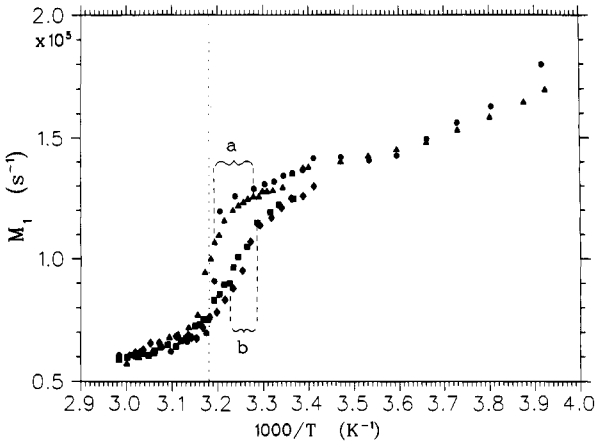

FIGURE 3: Temperature dependence of the first spectral moment, M_1, for multilamellar dispersions of [7,7,-$^2H_2$]DPPC with 0 (circles), 2 (triangles), 4 (squares), and 6% (diamonds) peptide-16 present. All moments were calculated from quadrupolar echo spectra, where $\tau_1 = 30$ μs. The two-phase regions for both the 2% and 4% peptide systems, are indicated by a and b, respectively. The temperature of the main phase transition is denoted by a dashed vertical line.

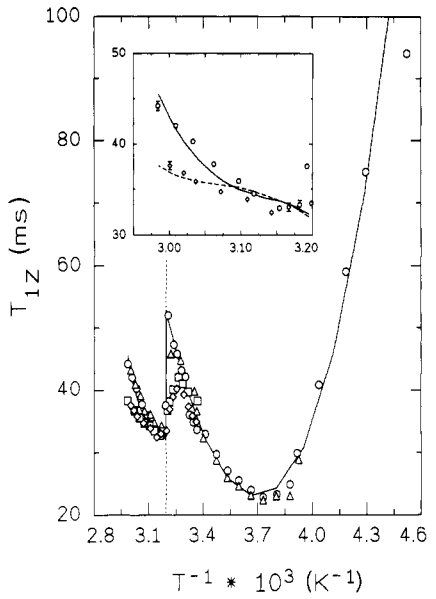

FIGURE 4: Temperature dependence of ^2H spin-lattice relaxation times, T_{1Z}, for multilamellar dispersions of [7,7,-$^2H_2$]DPPC with 0 (circles), 2 (triangles), 4 (squares), and 6% (diamonds) peptide-16 present. The powder averaged T_{1Z} was determined by measuring the areas under the spectra for each value of τ_2. The temperature of the main phase transition is denoted by a dashed vertical line. The T_{1Z} profile strongly depends on peptide concentration in the L_α phase. The fits for pure DPPC (solid line) and DPPC containing 6% peptide (dashed line) are included in the inset; also included are typical uncertainties in the estimates of T_{1Z}. In the gel phase at lower temperatures, the T_{1Z} values for DPPC–6%-Pep do not differ significantly from the ones for pure DPPC, and hence only the pure lipid fit is shown.

1985). The system containing 6% peptide is believed to exist outside the two-phase region (Morrow & Whitehead, 1988).

Relaxation Curves. Figure 4 shows spin-lattice relaxation times T_{1Z} for pure DPPC bilayers plotted as a function of inverse temperature. The relaxation times of the system containing 2% peptide are very similar to the pure lipid system. In contrast, the relaxation times of the 4% peptide system are markedly different from either the pure system or the 2% peptide system yet are very similar to those of the 6% system. The values show a significant discontinuity at T_M and a broad minimum at 268 K, similar to that observed by Mayer et al. (1988) in a closely related system. Following their interpretation, we therefore attribute this T_{1Z} minimum to the two-site jump of the *sn*-2 chain. In the inset of Figure 4, the measurements of the L_α phase of pure DPPC are shown. A continuous increase of the values with increasing temperatures is found. Analysis of the angular variation of T_{1Z} clearly shows that restricted rotational diffusion of the lipid molecules as a whole constitutes the dominant relaxation process above T_M (Mayer et al., 1990).

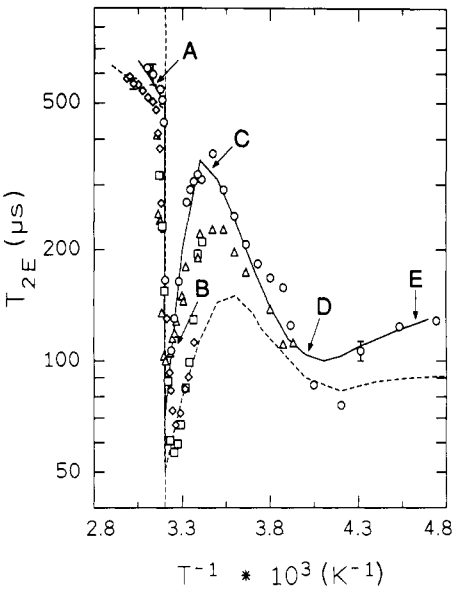

FIGURE 5: Temperature dependence of ^2H transverse spin relaxation times, T_{2E}, for multilamellar dispersions of [7,7,-$^2H_2$]DPPC with 0 (circles), 2 (triangles), 4 (squares), and 6% (diamonds) peptide-16 present. The temperature of the main phase transition is denoted by a dashed vertical line. The solid lines represent best fit simulations for the pure lipid, while the dashed lines represent best fit simulations for a system containing 6% peptide. Typical quadrupolar spectra from the various phases ($\tau_1 = 30$ μs) of the pure lipid system are shown in Figure 2. A, B, C, D, and E denote the temperatures at which these spectra were obtained.

In the gel phase at lower temperatures, the T_{1Z} values for DPPC–6%-Pep do not differ significantly from the ones for pure DPPC. In contrast, just below the main transition, the temperature dependence of T_{1Z} is strongly affected by the peptide. However, the biphasic character of this temperature region prevents an unambiguous analysis of the T_{1Z} data. Above T_M, the temperature dependence of T_{1Z} for DPPC–6%-Pep (Figure 4 (inset)) appears to be smaller than in the case of pure DPPC bilayers. This region was analyzed using, as a first approximation, the data found for the pure system.

In Figure 5, T_{2E} relaxation times for pure DPPC bilayers are plotted against inverse temperature (circles). On lowering the temperature, T_{2E} decreases in the L_α phase and drops to a very low value just below the main transition temperature at 311 K. This is consistent with observations of other lipid and protein–lipid systems in which the T_{2E} effective motions are thought to slow down abruptly at the main transition (Meier et al., 1986; Mayer et al., 1988). As the temperature is lowered, T_{2E} increases toward a maximum around 288 K. This rise in T_{2E} throughout the intermediate ($P_{\beta'}$) phase is accompanied by a corresponding increase in the T_{2E} anisotropy. At 311 K, there is no significant T_{2E} anisotropy whereas the ratio of T_{2E}, measured from the decay of the outer edge of the quadrupole echo spectra, to T_{2E} of the powder average reaches a value of 1.7 in the region of the T_{2E} maximum at 288 K. This unusual T_{2E} behavior can be rationalized by the existence of two lipid components below T_M (Mayer et al., 1988). The fraction of the motionally restricted component strongly increases with decreasing temperature. Thus, below 288 K only the high

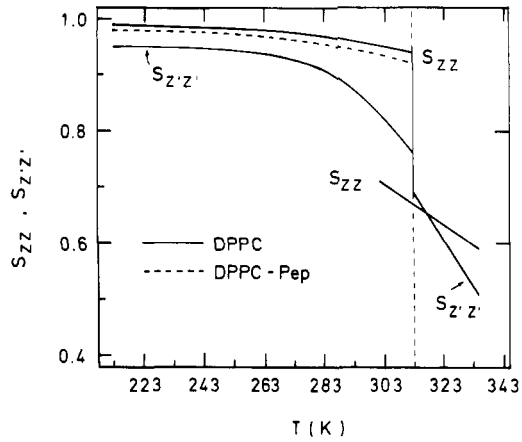

FIGURE 6: Temperature dependence of the segmental order parameter, $S_{Z'Z'}$, and the molecular orientational order parameter, S_{ZZ}, of pure multilamellar [7,7-$^2H_2$]DPPC (solid lines) and a system containing 6% peptide (dashed lines). The temperature of the main phase transition is denoted by a dashed vertical line.

order component is left. Lastly, T_{2E} passes through a minimum at 240 K; at this low temperatureminimum, long axis librations are presumed to become T_{2E} effective.

The corresponding result for the DPPC–6%-Pep system is also shown in Figure 5 (diamonds). Compared to the data of the pure system, two main differences can be established: First, as for T_{1Z}, the temperature dependence of T_{2E} in the L_α phase is more weakly expressed. Second, the sharp drop at the main transition is missing, being replaced by a steep but continuous decrease. This again reflects the broad two-phase region. The T_{2E} plot in Figure 5 was analyzed using the data of the pure DPPC system as starting values. Since measurements below 293 K are missing for the 6% peptide sample, this part of the analysis is merely an extrapolation based on parameters from the pure DPPC system. Generally all T_{2E} values are smaller for DPPC–6%-Pep below the main transition. As in the case of T_{1Z}, the continuous change of the relaxation times around T_M has not been analyzed quantitatively. In principle such an analysis can be achieved by assuming changing amounts of the two components coexisting in this region. However, because of the additional parameters involved, there is no unique fit.

Note from Figure 5 that for all peptide–lipid systems observed the T_{2E} maximum which occurred at 288 K for the pure lipid is much less pronounced. Furthermore, the strong T_{2E} anisotropy, observed throughout the $P_{\beta'}$ phase in the pure lipid, is virtually removed by the presence of 2, 4, or 6% peptide-16. Apparently the fraction of the restricted component is decreased by the presence of protein. This drastic disruption of the ripple phase by a small amount of peptide has been observed previously in similar systems (Kapitza et al., 1984) and is not surprising in light of the model of McCullough et al. (1990), where the formation of the ripple phase relies on a highly pure system of identical anisotropic molecules.

The temperature-dependent profiles of the first spectral moment for 0, 2, 4, and 6% peptide also corroborate the above two-component concept; the addition of peptide results in a decreased fraction of the (motionally restricted) "broad" spectral component and hence results in a decreased value of M_1. Note from Figure 3 that the M_1 profiles appear to converge at 288 K which corresponds to the temperature of the above-mentioned T_{2E} maximum.

A systematic analysis of the relaxation data yielded a set of temperature-dependent parameters describing order and dynamics of the bilayer structures, i.e., the order parameters of the lipid molecules (see Figure 6), the correlation times and

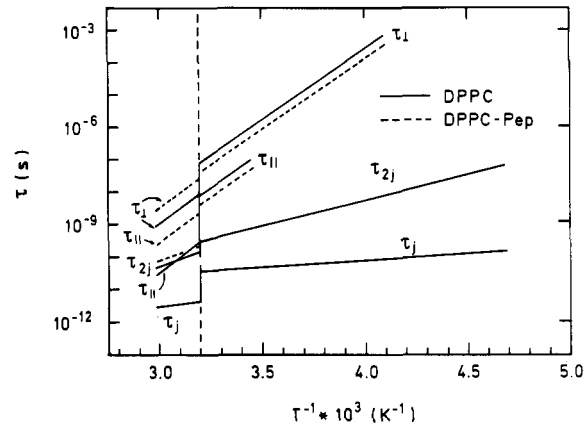

FIGURE 7: Arrhenius plots of various correlation times for whole body and internal molecular motions in pure multilamellar [7,7,-$^2H_2$]DPPC (solid lines) and a system containing 6% peptide (dashed lines). τ_j = correlation time for the isomerization process at the observed segment. τ_{2j} = correlation time for the two-site jump motion of the *sn*-2 chain. $\tau_{R_\parallel}$, $\tau_{R_\perp}$ = correlation times describing anisotropic rotational diffusion of the lipid molecule. The temperature of the main phase transition is denoted by a dashed vertical line.

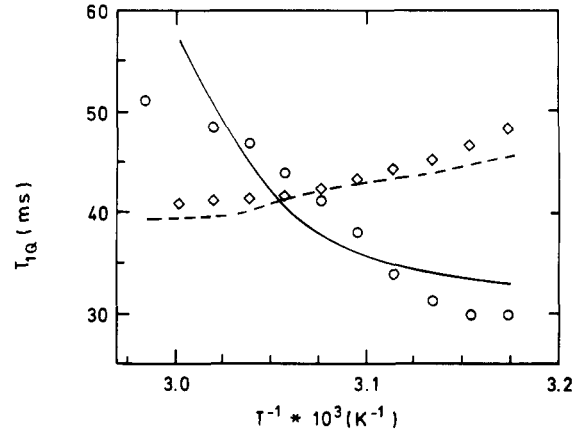

FIGURE 8: Temperature dependence of ^2H quadrupolar order relaxation times, T_{1Q}, in pure multilamellar [7,7,-$^2H_2$]DPPC (circles) and a system containing 6% peptide (diamonds), in the L_α phase. The solid and dashed lines represent extrapolations for the pure lipid and peptide containing system, respectively, based on the parameters obtained from the simulations of the inversion recovery and quadrupolar echo experiments.

activation energies of individual lipid motions (see Figure 7), and the viscoelastic parameters characterizing collective lipid motions (see eq 13). We have confined our analysis to pure DPPC bilayers and to DPPC containing 6% peptide (DPPC and DPPC–6%-Pep). Furthermore, since the gel phase T_{1Z} values appear to be independent of the peptide content, only one data set has been analyzed below T_M. Best fit simulations, represented by solid and dashed lines in Figures 4, 5, and 8, agree favorably with their experimental counterparts. Note that the temperature dependencies of T_{1Z}, T_{2E}, and T_{1Q} are reproduced with the same set of parameters, which are discussed in more detail in the following section.

Molecular Order. The molecular order in phospholipid bilayers comprises the orientational order of the lipid molecules with respect to the local director and the conformational order of the various chain segments. Figure 6 shows the temperature dependence of the orientational order parameter S_{ZZ}. This order parameter characterizes the "rigid body" order of the phospholipid molecules in the bilayer system. Generally the maximum error for S_{ZZ} is ±5% (Mayer et al., 1990). The solid line refers to pure DPPC bilayers, the dotted line to DPPC bilayers containing 6% peptide (DPPC–6%-Pep). The presence of peptide results in slightly reduced orientational

order throughout the $L_{\beta'}$ phase. The same applies, albeit to a lesser extent, in the L_α phase (not visible in Figure 6). Generally, S_{ZZ} continuously decreases with increasing temperature. The values in the liquid crystalline state are significantly lower than those in the gel phase. In the intermediate phase, two components, corresponding to motionally restricted and unrestricted lipids, are observed showing order parameters similar to those of the L_α and the $L_{\beta'}$ phases, respectively.

Figure 6 also includes the temperature dependence of the segmental order parameter, $S_{Z'Z'}$, which describes the conformational order of the individual chain segment. The addition of peptide does not appear to affect the segmental order parameter. Decreasing segmental order is observed with increasing temperature, showing a discontinuity at the main transition.

Local Lipid Motions. Local molecular dynamics are described in terms of motional correlation times characterizing the various motions. The internal motions consist of gauche–trans isomerizations of the observed chain segment (τ_j) and gauche–gauche isomerizations of the 2-segment leading to a two-site jump of the *sn*-2 chain (τ_{2_j}). The whole body motions include anisotropic rotational diffusion in an orienting potential described by two correlation times: $\tau_{R_\parallel}$ and $\tau_{R_\perp}$. Figure 7 is an Arrhenius plot of the various correlation times characterizing the motions in the pure DPPC and DPPC–6%-Pep bilayer (represented by solid and dashed lines respectively). All plots are linear within a particular phase, exhibiting more or less pronounced discontinuities at the main transition. The correlation times for restricted rotational diffusion show constant anisotropy ratios ($\tau_{R_\perp}/\tau_{R_\parallel}$) between 10 and 30, in the gel and liquid crystalline phases, respectively, and activation energies of 90 kJ/mol. In the case of the segmental motions, activation energies of 8 and 45 kJ/mol are observed in these phases, respectively. Rotational diffusion does not occur at temperatures much below the $P_{\beta'}$ phase. Rather, for $T < T_M$, molecular rotation (characterized by $\tau_{R_\parallel}$) gradually freezes out until only slow wobbling of the long molecular axis ($\tau_{R_\perp}$) can be detected.

Recently, a series of stochastic boundary molecular dynamics simulations of DPPC in a liquid crystalline membrane have been reported (De Loof et al., 1991; Pastor et al., 1991). These hybrid methods of molecular dynamics and Langevin dynamics provide very detailed information on the bilayer, while reaching times scales relevant to whole body motions. In one such simulation of DPPC at 324 K, Pastor et al. (1991) obtained estimates for the components of the lipid rotational diffusion tensor, $D_\perp \approx (1-2) \times 10^8$ s^{-1} and $D_\parallel \approx 2 \times 10^{10}$ s^{-1}, and average trans–gauche and gauche–trans isomerization rates for the central chain dihedral angles equal to 4×10^9 s^{-1} and 2×10^{10} s^{-1}, respectively. From an ensemble averaged cone angle, these authors also calculated an effective molecular order parameter, $S_W = 0.5$–0.7. Using the relations (Woessner et al., 1969)

$$D_\perp = \frac{1}{6\tau_{R_\perp}} \tag{9a}$$

$$D_\parallel = \frac{1}{6\tau_{R_\parallel}} \tag{9b}$$

we can compare the correlation times obtained from our model of totational diffusion in an orienting potential with the corresponding parameters of Pastor et al. (1991) for a model of wobble in a cone. Our results at 324 K are $D_\perp \approx 6 \times 10^7$ s^{-1} and $D_\parallel \approx 2 \times 10^9$ s^{-1} with $S_{ZZ} = 0.65$. Note that the theoretical anisotropy value ($D_\parallel/D_\perp \approx 130$) of Pastor et al. (1991) is significantly higher than our value of 30, although comparable to the experimentally derived anisotropy value found for DMPC/cholesterol systems (Weisz et al., 1991). Although our model for gauche–trans isomerizations is one of random rotational jumps, an average jump rate can be obtained according to

$$k_{eff} = (2\pi\tau_j)^{-1} \tag{10}$$

giving $k_{eff} = 4 \times 10^{10}$ s^{-1} in fair agreement with the average isomerization rate of $k \approx 1.3 \times 10^{10}$ s^{-1} predicted by Pastor et al.

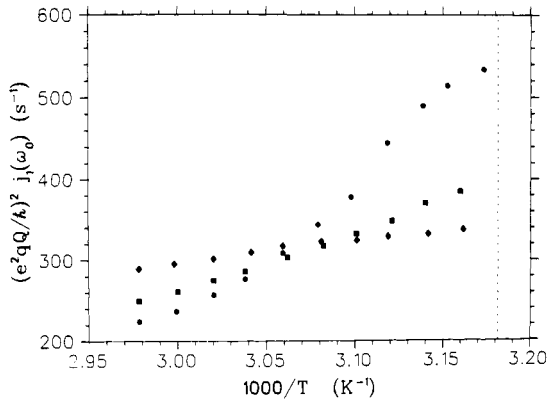

FIGURE 9: Temperature dependence of the reduced spectral density function, $j_1(\omega_0)$, obtained from values of T_{1Z} and T_{1Q} in the L_α phase. The systems displayed are pure multilamellar [7,7,-$^2H_2$]DPPC (circles), DPPC containing 4% peptide-16 (squares), and DPPC containing 6% peptide-16 (diamonds). The temperature of the main phase transition is denoted by a dashed vertical line.

The effect of the peptide on the internal motions seems to be marginal; only τ_{2_j} in the liquid crystalline phase is slightly increased. In contrast, the correlation times for restricted rotational diffusion in the L_α phase increase significantly. Note, however, that the anisotropy ratio ($\tau_{R_\perp}/\tau_{R_\parallel}$) is reduced. Below the main transition, both whole body correlation times decrease upon addition of the peptide. Apparently, integral peptides diminish the abrupt change of the whole body dynamics in pure lipid systems at the main transition.

As is illustrated by Figure 8, the presence of peptide causes a drastic change in the temperature-dependent profile of the characteristic relaxation time for quadrupolar order, T_{1Q}. Using only the parameters obtained from the simulations of the inversion recovery and quadrupolar echo experiments, we were able to reproduce the T_{1Q} profiles for both the pure lipid and the DPPC–6%-Pep system. Note the departure of T_{1Q} from the corresponding theoretical curve for the pure DPPC system at high temperatures in Figure 8. It is possible that lateral diffusion over curved surfaces during the variable time, τ_4, causes the relaxation time, T_{1Q}, to appear smaller; this effect would be most apparent at high temperatures where we expect a higher diffusion constant. In the Redfield limit, T_{1Q} is directly related to the reduced spectral density function $j_1(\omega_0)$ (Bloom et al., 1991):

$$1/j_1(\omega_0) = (9/8)(e^2qQ/\hbar)^2 k_1 T_{1Q} \tag{11a}$$

$$k_1 \approx (1/5)(1 - S_{CD}^2) \tag{11b}$$

$j_1(\omega_0)$ is displayed in Figure 9 as a function of inverse temperature and peptide concentration. Note that the addition of peptide results in a decrease in $j_1(\omega_0)$ at the low temperature end of the L_α phase and an increase in $j_1(\omega_0)$ at the high temperature end. Assuming there exists a single characteristic

correlation time τ_R at ω_0, i.e., $j_1(\omega_0) = \tau_R/(1 + \omega_0^2\tau_R^2)$, we expect an increase in peptide concentration (which would presumably cause an increase in τ_R) to increase $j_1(\omega_0)$ in some temperature range ($\tau_R < 1/\omega_0$) and to decrease $j_1(\omega_0)$ in a lower temperature range ($\tau_R > 1/\omega_0$). This is clearly observed in Figure 9. It follows that there will exist some temperature where $j_1(\omega_0)$ is essentially independent of peptide concentration (i.e., $\tau_R \sim 1/\omega_0 = 2.9$ ns at $1000/T = 3.07$ K^{-1}). From Figure 7 it can be seen that this characteristic correlation time corresponds closely to $\tau_{R\perp}$.

Collective Lipid Motions. So far we have focused on the motions of individual lipid molecules, which fully account for spin lattice relaxation in the conventional megahertz range. However, the short transverse relaxation times, observed above T_M (see Figure 5), cannot be described by fast molecular reorientations with correlation times of 10^{-7} s $> \tau_R > 10^{-12}$ s. Rather, low frequency motions with $\tau_R > 10^{-6}$ s are expected to contribute to the transverse relaxation at higher temperatures. Ample evidence for the occurrence of slow motions in the L_α phase of membranes comes from spin lattice relaxation studies in the kilohertz regime (Rommel et al., 1988) as well as from measurements of the transverse relaxation in quadrupole echo (Watnick et al., 1990a,b; Stohrer et al., 1991) and Carr–Purcell–Meiboom–Gill pulse sequences (Bloom and Sternin, 1987; Stohrer et al., 1991). From the anisotropy and pulse frequency dispersion of ^{2}H spin–spin relaxation times, observed for oriented DMPC bilayers, Stohrer et al. (1991) conclude that order director fluctuations represent the dominant transverse relaxation process in fluid membranes. The results of these authors also indicate only a small mean square displacement of the instantaneous director from its equilibrium configuration; assuming this to be the case in the systems we studied, the contributions of the collective order fluctuations to the measured order parameters S_{ZZ} (see Figure 6) are expected to be marginal.

The collective motion model also predicts a $\sin^2\xi\cos^2\xi$ dependence in $1/T_{2E}$ for proton decoupled spectra (Stohrer et al., 1991; Bloom & Evans, 1991); here ξ represents the angle between the external magnetic field and the bilayer surface normal. This T_{2E} anisotropy, which is reflected in the uncharacteristically large T_{2E} uncertainties in the L_α phase (see Figure 5), is apparently diminished with the successive addition of peptide-16. At 333 K, the ratio of T_{2E}, for $\xi = 90°$, to the powder averaged T_{2E}, is observed to gradually decrease from 1.63, for pure DPPC, to 1.28, in the presence of 6% peptide-16; this same ratio correspondingly decreases from 1.53 to 1.41 at 323 K. $\sigma_{R_\parallel}$ and $\tau_{R_\perp}$ both increase significantly with the addition of peptide (see Figure 7). Larger values of these correlation times imply that the contribution of the overall lipid motion to T_{2E} will be increased and the T_{2E} anisotropy correspondingly reduced (Weisz et al., 1991).

Although collective order fluctuations occur in the low frequency realm (Rommel et al., 1988), there may also be high frequency contributions to T_{2E} since (Vold, 1985)

$$1/T_{2E} = (3/16)(e^2qQ/\hbar)^2[3J_0(0) + 3J_1(\omega_0) + 2J_2(2\omega_0)] \quad (12)$$

Therefore when discussing collective order fluctuations, it is preferable to remove these high frequency contributions and compare the temperature dependence of $J_0(0)$. In the model described by Stohrer et al. (1991), $J_0(0)$ depends on the effective viscosity of the fluid medium, η, the C–D bond order parameter, S_{CD}, the effective elastic constant of the membrane,

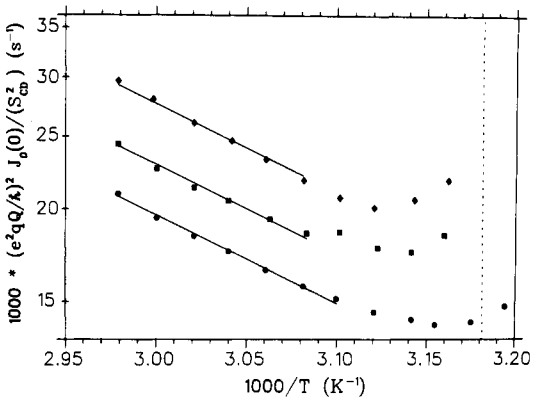

FIGURE 10: Temperature dependence of the scaled spectral density function, $J_0(0)/S_{CD}^2$, obtained from values of T_{1Z}, T_{2E}, and T_{1Q} in the L_α phase. The systems displayed are pure multilamellar [7,7,-^{2}H$_2$]-DPPC (circles), DPPC containing 4% peptide-16 (squares), and DPPC containing 6% peptide-16 (diamonds). Above the temperature where phase transition effects occur, there appears to be a region where $J_0(0)/S_{CD}^2$ is linear as a function of inverse temperature (solid lines).

K, the average bilayer thickness, d, and the long wavelength cutoff of the elastic modes, λ_l, such that

$$J_0(0) \propto S_{CD}^2[k_BT\eta\lambda_l^2/(K^2d)] \quad (13)$$

In Figure 10, the scaled spectral density function $J_0(0)/S_{CD}^2$ is displayed as a function of inverse temperature and peptide concentration. There is a consistent and uniform increase in $J_0(0)/S_{CD}^2$ upon addition of peptide in the L_α phase. Assuming that η and λ_l do not change significantly in going from pure lipid to 6% peptide, and noting work by Huschilt et al. (1985), with perdeuteriated DPPC, which revealed the first spectral moment, M_1 (which is directly related to the bilayer thickness), to be relatively independent of peptide-16 concentration in the L_α phase, we obtain the membrane elastic constant, K, as the only variable. From Figure 10, there appears to be a linear temperature dependence of $J_0(0)/S_{CD}^2$ for the pure lipid and peptide–lipid systems, above the temperature where phase transition effects occur. From the differences of the y-intercepts of the lines defining $J_0(0)/S_{CD}^2$ vs T for each of the systems (see Figure 10), we conclude that the elastic constant is 0.92 and 0.84 times that of the elastic constant of the pure lipid system, for the 4% and 6% peptide systems, respectively. This suggests that there is a significant enhancement of collective lipid motions upon the addition of an integral peptide.

Watnick et al. (1990a) have briefly reviewed the relevance of collective motions to biological function; it is significant that an enhancement of collective motions results even though there is no hydrophobic mismatch between the lipid and peptide. This result may be compared to that of Weisz et al. (1991) in which the average membrane elastic constant was observed to increase upon the addition of cholesterol. Cholesterol is known to inhibit the amplitude of lipid chain libration and decrease the fraction of gauche conformers, while peptide seem to have the opposite effect; these microscopic properties may be directly related to the average elastic constant.

CONCLUSIONS AND FUTURE PROSPECTS

We have studied the influence of an integral membrane peptide on phospholipid order and dynamics over a broad temperature range encompassing the liquid crystalline, intermediate, and gel phases. Analysis of the experiments, employing a density matrix treatment based on the stochastic Liouville equation, revealed information above the dynamic organization of the lipid in the different membrane phases.

This dynamic organization is described in terms of segmental and orientational order parameters and in terms of correlation times corresponding to both internal and whole body lipid motions. Generally, the results for DPPC were found to be remarkably similar to those reported by Mayer et al. (1988) for DMPC.

In the liquid crystalline phase, the orientational order parameter, S_{ZZ}, was observed to decrease slightly upon addition of peptide while the order parameter corresponding to the seventh segment, $S_{Z'Z'}$, did not change at all for any concentration of peptide. In general, the gauche–trans isomerization rate in the middle of the chain was not observed to change upon the addition of peptide, whereas the whole body reorientational correlation times ($\tau_{R_\parallel}$ and $\tau_{R_\perp}$) increased by nearly an order of magnitude. The anisotropy ratio ($\tau_{R_\perp}/\tau_{R_\parallel}$) decreased with peptide added. An additional motion which involves a jump about the axis of the *sn*-2 chain is also observed to be slowed down significantly by peptide. Assuming T_{2E} is dominanted by collective order director fluctuations in the liquid crystalline phase, we conclude that peptide decreases the effective membrane elastic constant. Some of the largest effects of the peptide on the dynamic organization of the lipid were found in the region of the intermediate phase. These effects were discussed in terms of recent statistical mechanical models of the ripple phase. In the gel state, the jumping process of the *sn*-2 chain is observed to slow down slightly while the whole body reorientational correlation times decrease with peptide added.

By analyzing the change in the reduced spectral density function, $j_1(\omega_0)$, as a function of temperature and peptide concentration, we argued that there should exist a motion whose characteristic correlation time was equal to 2.9 ns at $1000/T = 3.07$ K^{-1}; this was in agreement with the value of the correlation time, $\tau_{R_\perp}$, obtained from the simulations. In the liquid crystalline phase, we were able to further validate the uniqueness of our evaluated parameters by reproducing the T_{1Q} profiles for both the pure lipid and the DPPC–6%-Pep system, using only the parameters obtained from the simulations of the inversion recovery and quadrupolar echo experiments. Lastly, the results of stochastic boundary molecular dynamics simulations of DPPC in the liquid crystalline phase (De Loof et al., 1991; Pastor et al., 1991) were in reasonable agreement with our findings, although the two-site jump could not be compared.

Finally, we would like to comment that the dependence of most of the order and relaxation parameters on peptide concentration appeared to be strongly nonlinear. We suggest that a careful study of some of these parameters as a function of many peptide concentrations would be useful to understand this potential nonlinearity.

ACKNOWLEDGMENT

Our thanks to Bob Hodges (University of Alberta, Canada) for synthesizing the peptide and to Dr. R. W. Pastor (Center for Biologics Evaluation and Research, Bethesda, MD) for helpful discussions.

REFERENCES

Bloom, M., & Sternin, E. (1987) *Biochemistry 26*, 2101–2105.
Bloom, M., & Evans, E. (1991) in *Biologically Inspired Physics* (Peliti, L., Ed.) Plenum Press, New York.
Bloom, M., Morrison, C., Sternin, E., & Thewalt, J. L. (1991) in *Pulsed Magnetic Resonance: NMR, ESR and Optics, a Recognition of E. L. Hahn* (Bagguley, D. M. S., Ed.) Oxford University Press, Oxford.
Carlson, J. M., & Sethna, J. P. (1987) *Phys. Rev. A 36*, 3359–3374.
Cotter, M. A. (1977) *J. Chem. Phys. 66*, 1098–1106.
Davis, J. H. (1983) *Biochim. Biophys. Acta.* 737, 117–171.
Davis, J. H., Clare, D. M., Hodges, R. S., & Bloom, M. (1983) *Biochemistry 22*, 5298–5305.
de Gennes, P. G. (1974) *The Principles of Liquid Crystals*, Clarendon Press, Oxford.
De Loof, H., Harvey, S., Segrest, J., & Pastor, R. (1991) *Biochemistry 30*, 2099–2113.
Freed, J. H. (1977) *J. Chem. Phys. 66*, 4183–4199.
Freed, J. H., Bruno, G. V., & Polnaszek, C. F. (1971) *J. Phys. Chem. 75*, 3385–3399.
Gupta, C. M., Radhakrishman, R., & Khorana, H. G. (1977) *Proc. Natl. Acad. Sci. U.S.A. 74*, 4315–4319.
Huschilt, J. C., Hodges, R. S., & Davis, J. H (1985) *Biochemistry 24*, 1377–1386.
Kapitza, H. G., Ruppel, D. A., Galla, H. J., & Sackmann, E. (1984) *Biophys. J. 45*, 577–587.
Kothe, G. (1977) *Mol. Phys. 33*, 147–158.
Kubo, R. (1969) *Stochastic Processes in Chemical Physics, Advances in Chemical Physics* (Shuler, K. E., Ed.) pp 101–127, Wiley Press, New York.
Marqusee, J. A., Warner, M., & Dill, K. A. (1984) *J. Chem. Phys. 81*, 6404–6405.
Mayer, C. Müller, K., Weisz, K., & Kothe, G. (1988) *Liq. Cryst. 3*, 797–806.
Mayer, C., Gröbner, G., Müller, K., Weisz, K., & Kothe, G. (1990) *Chem. Phys. Lett. 165*, 155–161.
McCullough, W. S., Perk, J. H. H., & Scott, H. L. (1990) *J. Chem. Phys. 93*, 6070–6080.
Meier, P., Ohmes, E., Kothe, G., Blume, A., Weidner, J., & Eibl, H. J. (1983) *J. Chem. Phys. 87*, 4904–4912.
Meier, P., Ohmes, E., & Kothe, G. (1986) *J. Chem. Phys. 85*, 3598–3614.
Moro, G., & Freed, J. H. (1981) *J. Chem. Phys. 74*, 3757–3773.
Morrow, M. R., & Whitehead, J. P. (1988) *Biochim. Biophys. Acta 941*, 271–277.
Müller, K., Meier, P., & Kothe, G. (1985) *Prog. Nucl. Magn. Reson. Spectrosc. 17*, 211–239.
Norris, J. R., & Weissman, S. I. (1969) *J. Phys. Chem. 73*, 3119–3124.
Pastor, R., Venable, R., & Karplus, M. (1991) *Proc. Natl. Acad. Sci. U.S.A. 88*, 892–896.
Pauls, K. P., MacKay, A. L., Söderman, O., Bloom, M., Tanjae, A. K., & Hodges, R. S. (1985) *Eur. Biophys. J. 12*, 1–11.
Pincus, P. (1969) *Solid State Commun. 7*, 415–417.
Redfield, A. G. (1965) *Adv. Magn. Reson. 1*, 1–32.
Rommel, E., Noack, F., Meier, P., & Kothe, G. (1988) *J. Phys. Chem. 92*, 2981–2987.
Saupe, A. (1964) *Z. Naturforsch. 19A*, 161–171.
Schneider, M. B., Chan, W. K., & Webb, W. W. (1983) *Biophys. J. 43*, 157–165.
Schwartz, L. J., Stillman, A. E., & Freed, J. H. (1982) *J. Chem. Phys. 77*, 5410–5425.
Sillescu, H. (1971) *J. Chem. Phys. 54*, 2110–2119.
Siminovitch, D. J., Ruocco, M. J., Olejniczak, E. T., Das Gupta, S. K., & Griffin, R. G. (1988) *Biophys. J. 54*, 373–381.
Stamatoff, J., Feuer, B., Guggenheim, H. J., Tellez, G., & Yamane, T. (1982) *Biophys. J. 38*, 217–226.
Stohrer, J., Gröbner, G., Reimer, D., Weisz, K., Mayer, C., & Kothe, G. (1991) *J. Chem. Phys. 95*, 672–678.
Vold, R. R. (1985) in *Nuclear Magnetic Resonance of Liquid Crystals* (Emsley, J. W., Ed.) pp 253–288, D. Reidel Publishing Co., Dordrecht.
Watnick, P., Dea, P., & Chan, S. (1990a) *Proc. Natl. Acad. Sci. U.S.A. 87*, 2082–2986.
Watnick, P., & Chan, S., & Dea, P. (1990b) *Biochemistry 29*, 6215–6221.
Weisz, K., Gröbner, G., Mayer, C., Stohrer, J., & Kothe, G. (1992) *Biochemistry 31*, 1100–1112.
Wittebort, R. J., Schmidt, C. F., & Griffin, R. G. (1981) *Biochemistry 20*, 4223–4228.
Woessner, D. E., Snowden, B. S., Jr., & Meyer, G. H. (1969) *J. Chem. Phys. 52*, 2968–2976.

Registry No. DPPC, 63-89-8; peptide-16, 94751-61-8.